Front. Environ. Sci. Eng. 2023, 17(3): 30
https://doi.org/10.1007/s11783-023-1630-3

RESEARCH ARTICLE

Nonpolar cross-stacked super-aligned carbon nanotube membrane for efficient wastewater treatment

Shuang Zhang[1,2], Shuai Liang (✉)[1,2], Yifan Gao[3], Yang Wu[4], Xia Huang[3]

1 Beijing Key Laboratory for Source Control Technology of Water Pollution, College of Environmental Science and Engineering, Beijing Forestry University, Beijing 100083, China
2 Engineering Research Center for Water Pollution Source Control & Eco-remediation, College of Environmental Science and Engineering, Beijing Forestry University, Beijing 100083, China
3 State Key Joint Laboratory of Environment Simulation and Pollution Control, School of Environment, Tsinghua University, Beijing 100084, China
4 Department of Physics and Tsinghua-Foxconn Nanotechnology Research Center, Tsinghua University, Beijing 100084, China

HIGHLIGHTS

- A novel nonpolar super-aligned carbon nanotube (SACNT) membrane was prepared.
- SACNT membranes achieved smoother and more uniform structures.
- SACNT membranes have inert chemistry and unique nonpolar wetting feature.
- SACNT membranes exhibit superior separation and antifouling capabilities.
- SACNT membranes achieved superior oil/water separation efficiency.

GRAPHIC ABSTRACT

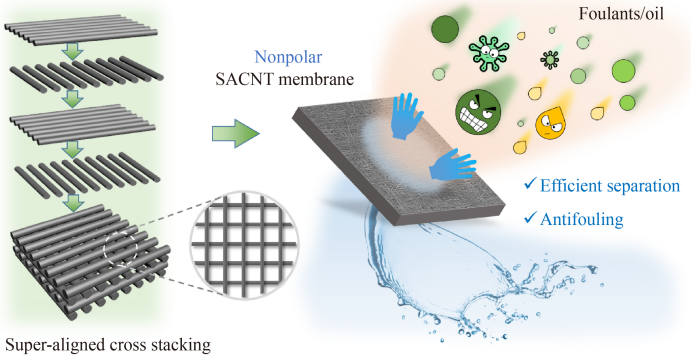

ARTICLE INFO

Article history:
Received 11 July 2022
Revised 9 August 2022
Accepted 12 August 2022
Available online 15 September 2022

Keywords:
Membrane fouling
Wastewater
Membrane separation
Antifouling
Aligned carbon nanotube

ABSTRACT

Membrane separation technology has made great progress in various practical applications, but the unsatisfactory separation performance of prevailing membrane materials hampers its further sustainable growth. This study proposed a novel nonpolar super-aligned carbon nanotube (SACNT) membrane, which was prepared with a layer-by-layer cross-stacking method. Through controlling the number of stacked SACNT layers, three kinds of SACNT membranes (SACNT_200, SACNT_300, and SACNT_400) were prepared. Systematic characterizations and filtration tests were performed to investigate their physico-chemical properties, surface wetting behavior, and filtration performance. Compared with two commercial membranes (Com_0.22 and Com_0.45), all the SACNT membranes achieved smoother and more uniform structures. Due to the hexagonal graphene structure of CNTs, the surface chemistry of the SACNT membranes is simple and inert, thereby potentially eliminating the covalent-bonding-induced membrane fouling. Besides, the SACNT membranes exhibited a typical nonpolar wetting behavior, with high contact angles for polar liquids (water: ~124.9°–126.5°; formamide: ~80.0°–83.9°) but low contact angles for nonpolar diiodomethane (~18.8°–20.9°). This unique nonpolar feature potentially leads to weak interactions with polar substances. Furthermore, compared with the commercial membranes, the SACNT membranes obtained a significantly higher selectivity while achieving a comparable or higher permeability (depending on the number of stacked layers). Moreover, the SACNT membranes exhibited superior separation performance in various application scenarios, including municipal wastewater treatment (> 2.3 times higher cleaning efficiency), electro-assistant fouling inhibition (or even self-cleaning), and oil/water separation (> 99.2 % of separation efficiency), suggesting promising application prospects in various fields.

✉ Corresponding author
E-mail: shuai_liang@bjfu.edu.cn

1 Introduction

Wastewater reclamation is an important measure to alleviate the global water crisis (Racar et al., 2020; Zhida Li, 2022). Compared with conventional water treatment technologies, membrane separation technology has been widely recognized as a more advantageous technology owing to its high treatment efficiency, low footprint, reliable effluent quality, and so forth (Wei et al., 2021; Liu et al., 2022). Micro-/ultra-filtration, as the most widely used membrane technology, has made great progress in practical applications in recent decades (Xiao et al., 2019). However, its further sustainable growth has been hampered due to membrane fouling (Wei et al., 2021; Li et al., 2022; Ma et al., 2022), which are closely related with the unsatisfactory separation performance of the prevailing membrane materials (Jiang et al., 2022; Xiong et al., 2022).

The prevailing commercial micro-/ultra-filtration membranes are mainly prepared using polar polymers based on phase-separation-based methods (e.g., non-solvent induced, thermally induced) (Qin et al., 2014; Hu et al., 2018), which normally result in pore-shaped structures. To maximize porosity and improve membrane selectivity, additional additives are commonly employed during membrane fabrication, thereby endowing the membrane with complex surface chemistry thus complicated interfacial interactions (Su et al., 2016; Zhao et al., 2018). Although great efforts have been made in the recent decades to improve the antifouling performance via various modification strategies (i.e., surface coating, matrix blending, surface grafting) (Li et al., 2019; Zin et al., 2019), but the obtained membranes commonly possess more complicated surface chemistry (Zhao et al., 2018), which is unfavorable for membrane fouling control (Wang et al., 2022). To improve the sustainability of membrane separation technology, further effort is needed to explore novel membrane materials, develop highly controllable fabrication strategies, reveal interfacial interaction mechanisms, and so on (Abaie et al., 2021; Jia et al., 2022).

Looking into the practical scenario of membrane-based wastewater treatment, it can be found that most substances that contact with membrane in the aqueous environment are polar. It has been well established that the polarity of molecules essentially determines their molecular interaction behaviors (van Oss, 2006). The polar–polar interaction is normally strong and associated with high affinity. The nonpolar–nonpolar interaction is weak but also associated with high affinity. The polar–nonpolar interaction is commonly weak and with low affinity. Therefore, considering the polar circumstances that a membrane normally faces in wastewater treatment, a nonpolar membrane may exhibit advantages in antifouling, because its near zero electric dipole moment is not conducive to the deposition of pollutants on the membrane surface (van Oss, 2006). However, such fundamental interaction mechanism is rarely considered in the previous membrane fabrication and modification studies. Also, nonpolar materials have not been sufficiently concerned in previous membrane preparation studies. Although carbon nanotube (CNT, a typical nonpolar material) had been increasingly employed for membrane fabrication (Sun et al., 2022a), the potential beneficial effects of its nonpolar feature had been barely investigated. Besides, in the field of water treatment, freestanding CNT membranes are commonly prepared via pressure-driven random deposition strategies, resulting in disordered and less-controllable membrane structures (Ihsanullah, 2019; Wang et al., 2020). A few studies developed vertically aligned CNT membranes (primarily for desalination or gas separation applications) (Ihsanullah, 2019; Lee et al., 2020), but they are not suitable for micro-/ultra-filtration processes due to limited pore size and porosity (Wang et al., 2020). Considering the above, a nonpolar CNT membrane with ordered and controllable structures may exhibit superior performance in water treatment processes.

In this study, a nonpolar super-aligned CNT (SACNT) membrane was prepared with a layer-by-layer cross-stacking strategy. Through controlling the number of stacked SACNT layers, three kinds of SACNT membranes corresponding with 200, 300, and 400 layers were prepared. Two types of commercial polyvinylidene fluoride (PVDF) membranes with nominated pore sizes of 0.22 and 0.45 μm were used as controls for comparison. Systematic characterizations were performed to investigate the physico-chemical properties, surface wetting behavior, and filtration performance (in terms of water permeability and selectivity) of the membranes. A series of filtration tests were also conducted to evaluate their antifouling and oil/water separation capabilities.

2 Materials and methods

2.1 Fabrication of cross-stacked SACNT membranes

The SACNT membranes were prepared with a layer-by-layer cross-stacking strategy. As shown in Fig. 1, an array of CNTs was first synthesized on a silicon wafer through pyrolysis of acetylene using iron as the catalyst with a low-pressure chemical vapor deposition system. Then a group of CNTs at the edge was draw out from the SACNT array. These CNTs were connected end to end owing to Van der Waals forces (Liu et al., 2011), thereby forming a monolayer of SACNT yarns. Immediately, this layer of SACNT was placed on a nonwoven polyethylene terephthalate fabric (Ahlstrom-Munksjö, Finland). To

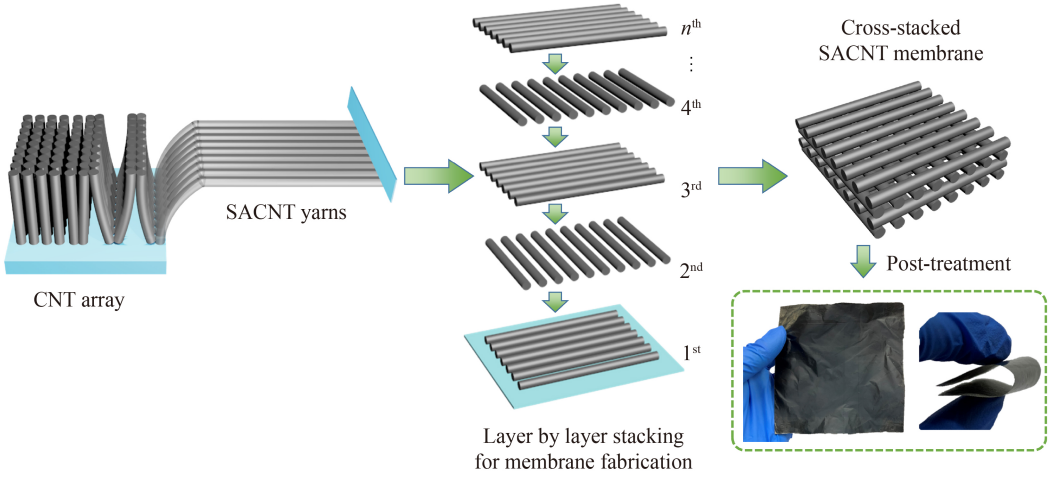

Fig. 1 Schematic illustrating the fabrication process of the super-aligned carbon nanotube (SACNT) membrane via a layer-by-layer cross-stacking strategy. Photographs of a prepared flexible and self-supported membrane are included.

prepare the SACNT membrane, multiple such SACNT layers were successively stacked in orthogonal directions. In this study, three kinds of SACNT membranes separately containing 200, 300, and 400 SACNT layers were prepared. They were hereafter designated as SACNT_200, SACNT_300, and SACNT_400 membranes, respectively. The resulted membranes were then sequentially soaked in ethanol for 30 min, air-dried, and stocked at room temperature (23 ± 1 °C). For comparative investigations, two kinds of commercial PVDF membranes with nominal average pore sizes of 0.22 μm (GVWP, Millipore, USA) and 0.45 μm (HVLP, Millipore, USA) were selected as controls. They were hereafter designated as Com_0.22 and Com_0.45 membranes, respectively.

2.2 Membrane characterizations

Membrane samples were air-dried at room temperature (23 ± 1 °C) prior to characterizations. Membrane surface morphology was observed by a field emission scanning electron microscope (FE-SEM, JSM-7001F, Hitachi, Japan). Prior to the observation, a 10-nm-thick platinum layer was sputter-coated on the samples to ensure good conductivity. An energy dispersive X-ray spectroscopy (EDS) unit equipped with the SEM system was employed to determine the elemental compositions of membrane surfaces. Surface functional groups were determined by attenuated total reflectance Flourier transform infrared spectroscopy (ATR-FTIR, VERTEX 70, Bruker, Germany).

Membrane surface roughness was characterized in terms of three parameters: root-mean-square roughness (R_{RMS}), maximum roughness (R_{max}), and average roughness (R_a), through an atomic force microscope (AFM, MFP-3D, Asylum Research, USA) in a tapping mode. For each membrane type, each final result was an average of at least nine measurements on three separately prepared membranes.

2.3 Evaluation of surface wetting property

Membrane surface contact angles with three different liquids, including deionized (DI) water (polar), formamide (polar, ⩾ 99.5 %, Sigma–Aldrich), and diiodomethane (nonpolar, 95 %, Aladdin, China), were measured to evaluate the wetting properties of the membranes. A video-supported measuring device (OCA 20, Dataphysics, Germany) was used to measure the contact angles. For each sample, the process of a 2.00 μL droplet of the test liquid (i.e., water, formamide, or diiodomethane) dropping on the membrane surface was recorded as a video. The instantaneous frame at ~0.3 s after the vibration of the liquid droplet stopped was used for contact angle fitting and calculation. For each membrane type, the final result was averaged from at least twelve measurements on randomly selected locations of at least two separately prepared membranes.

2.4 Evaluation of membrane permeability and selectivity

A semi-dead-end filtration cell (Amicon 8010, Millipore, USA; see setup diagram in Fig. S1) was employed to carry out a series of filtration tests for the evaluation of membrane water permeability and selectivity. For permeability measurements, a 3 h filtration operation with DI water was performed at ~10 kPa. The permeability (m/(s·kPa)) can be calculated based on the continuously recorded mass of the permeate (Ma et al., 2020). The data from the last 10 min (when the membrane could be considered as sufficiently compressed in the previous 170 min filtration) were averaged and determined as the final permeability result.

To evaluate membrane selectivity, the membrane

sample was subsequently used for molecular weight cut off (MWCO) tests. A series of filtration operations were sequentially carried out using different poly (ethylene oxide) (PEO) solutions (1 g/L) with increasing molecular weights (100, 200, 300, 400, and 600 kDa). For each filtration operation, the total organic carbon (TOC) of the permeate and residual feed solution were determined (TOC-VCSH, Shimadzu, Japan), and the rejection rate (ψ) corresponding to a certain molecular weight can be calculated as:

$$\psi = 1 - \frac{C_e}{C_f}, \quad (1)$$

where the C_e and C_f are the TOC concentrations of the effluent and feed solution, respectively. The MWCO of a membrane is defined as the lowest molecular weight at which 90 % rejection is reached.

2.5 Evaluation of antifouling performance for municipal wastewater treatment

A series of three-cycle filtration tests using synthetic municipal wastewater (Table 1, determined according to a previously published study (Shen et al., 2012)) as feed were performed to assess the antifouling performance of the prepared membranes. Three typical organic model foulants, including bovine serum albumin (Sigma–Aldrich), sodium alginate (Aldrich), and humic acid (Aldrich), were used as representatives of proteins, polysaccharides, and natural organic matter, respectively. A set of inorganic substances including $CaCl_2$/$MgCl_2$, NaCl, and $NaHCO_3$ were used to provide water hardness, adjust ionic strength, and buffer solution pH, respectively.

The same semi-dead-end filtration system used for the permeability and MWCO tests was employed in the three-cycle antifouling filtration tests. Each three-cycle filtration operation comprises alternated fouling filtration, permeability test, and membrane cleaning procedures. The fouling filtration was carried out using the synthetic foulant solution as feed at a transmembrane pressure (TMP) of 10 kPa and a stirring rate of 100 r/min for 24 h. The permeability test was performed before and after the membrane cleaning using DI water as feed at 10 kPa and 100 r/min for ~2 h. The membrane cleaning was conducted on site with DI water by increasing the stirring rate to 200 r/min for 5 min. The enhanced shearing force was expected to rinse the adsorbed foulants off the membrane. The cleaning efficiency (η) for each cycle can be calculated as:

$$\eta = \frac{J_C - J_F}{J_0 - J_F}, \quad (2)$$

where the J_0, J_F, and J_C indicate the permeability measured with DI water of the pristine, fouled, and cleaned membranes, respectively.

Table 1 Chemistry of the synthetic municipal wastewater

Items	Component	Concentration
Organic (mg/L)	Sodium alginate	20
	Humic acid	10
	Bovine serum albumin	10
Inorganic (mmol/L)	$CaCl_2$	1
	$MgCl_2$	0.5
	$NaHCO_3$	2
	NaCl	9

2.6 Evaluation of electro-assistant antifouling performance

The electrically conductive property of the SACNT membrane potentially enables an electro-assistant antifouling capability (Li et al., 2020; Hand and Cusick, 2021; Wei et al., 2021), which was assessed through a set of filtration tests with an electrically-enhanced cross-flow filtration system (Fig. S2). During filtration, a 1 V voltage was applied between the SACNT membrane (cathode) and a titanium foil (anode) with an electrochemical workstation (CHI650E, CH Instruments, Inc., USA). Peristaltic pumps (BT100-1F, Longer Pump, China) were used to drive the feed solution (synthetic foulant solution, Table 1) flow into the chamber between the membrane and titanium foil (1 mm apart), and pass through the membrane (1.6 cm × 5 cm, i.e., 8 cm^2 of effective filtration area). TMPs were recorded as antifouling indexes to assess the antifouling performance of the SACNT membrane.

2.7 Evaluation of oil-water separation performance

A surfactant-stabilized oil-in-water emulsion was prepared through mixing 10 mL of soybean oil/sodium dodecyl sulfate (9:1, w/w) mixture in 1 L of DI water under vigorous stirring and ultrasonication treatment (KQ5200E, Kunshan Ultrasonic Instruments, China) for 30 min. The resulted emulsions could remain stable for at least one week. The average oil particle size was measured to be 5.375 μm using a laser diffraction particle size analyzer (Mastersizer 2000, Malvern Co., UK).

A three-cycle filtration experiment was performed to investigate the oil/water separation behaviour of the membrane using the same semi-dead-end filtration system used for the permeability and MWCO tests. For each cycle, the oil-in-water emulsion was introduced to the stirred (200 r/min) filtration cell, and the filtration was carried out at a constant pressure of 3 kPa for 1 h. Afterwards, the membrane was cleaned on site with DI water by increasing the stirring rate to 400 r/min for 5 min. All the effluent in the three-cycle filtration was collected and mixed for concentration measurement with an ultraviolet spectrometer (UVS, UV-5200, Shanghai Metash Instruments, China). The oil rejection rate (r) can

be calculated as:

$$r = \frac{A_F - A_E}{A_F}, \quad (3)$$

where the A_F and A_E refer to the absorbance of the feed emulsion and effluent, respectively.

3 Results and discussion

3.1 Membrane surface morphology and chemistry

As presented in Fig. 1, the prepared SACNT membrane is self-supported and highly flexible. Macroscopically, all of the membranes look smooth and reflective. Microscopically (Figs. 2(a)–2(c)), all of the SACNT membranes possess a vertically staggered nanofiber-based structure, which is significantly different from the random distribution structure of conventional CNT membranes prepared by conventional methods (e.g., vacuum filtration (Yang et al., 2019; Zhang et al., 2020a; Wei et al., 2021), Fig. S3). The uniform and highly controllable structure can be recognized as a characteristic feature of the SACNT membranes. Another feature is the length and continuity of each nanotube, which potentially improves the integrity and mechanical strength of the SACNT membrane (Zhu et al., 2018).

The morphology of the SACNT membrane is also significantly different from those of the prevailing commercial microfiltration/ultrafiltration membranes, which are normally prepared with phase-separation-based methods (Ma et al., 2020). As shown in Fig. 2(d) (Com_0.22) and Fig. 2(e) (Com_0.45), the phase separation process normally brings about "pore" structures. But the SACNT membranes do not have clear "pore" morphology on their surfaces. The difference in membrane structure and morphology results in different separation behaviors, which will be discussed later.

The EDS analyses demonstrate that the SACNT membrane is mainly composed of carbon element. This verifies that the nanotubes in the SACNT membranes are CNTs. By contrast, the Com_0.22 and Com_0.45 membranes mainly comprise C, F, N, and O elements. The C and F should be attributed to the matrix PVDF material, while the N and O can be ascribed to the additives added during fabrication for improvement of membrane porosity and hydrophilicity (Ma et al., 2020).

As for surface roughness (Fig. 3), the SACNT membranes are observed to be much smoother than the Com_0.22 and Com_0.45 membranes. Taking R_a as a representative Roughness parameter, the measured R_a of the SACNT_200, SACNT_300, and SACNT_400 membranes are 67.0 ± 3.7, 73.8 ± 19.9, and 43.9 ± 2.9 nm, respectively. In marked contrast, the R_a of the Com_0.22 and Com_0.45 membranes are measured to be 330.0 ± 27.3 and 304.3 ± 17.0 nm, respectively. Approximately, the commercial membranes are five times rougher than the SACNT membranes. Considering that a rough surface might tend to stuck foulants, the smooth feature of the SACNT membrane may be favorable for mitigation of membrane fouling (Wang et al., 2022; Zhao et al., 2022) (further discussed later). Besides, it is noteworthy that stacking more SACNT layers did not bring about significant changes in surface morphology.

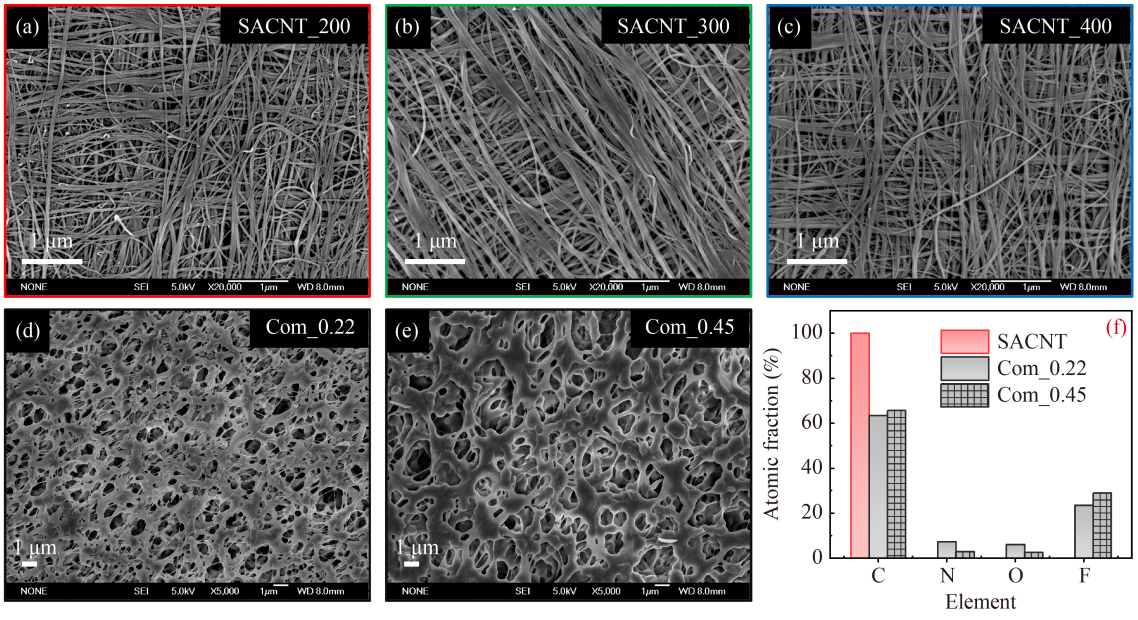

Fig. 2 SEM top views of the (a) SACNT_200, (b) SACNT_300, (c) SACNT_400, (d) Com_0.22 PVDF, and (e) Com_0.45 PVDF membranes. (f) Comparison of elemental compositions among the typical SACNT membrane (taking SACNT_200 as a representative) and commercial membranes.

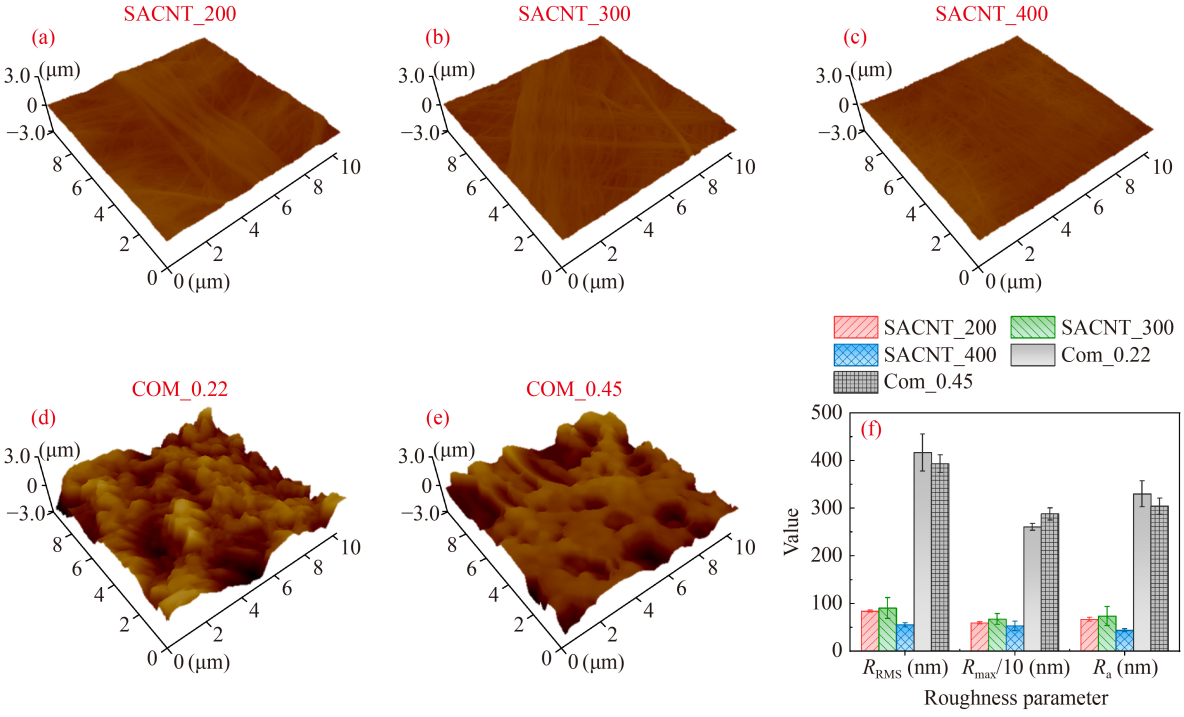

Fig. 3 Surface morphology by AFM of the (a) SACNT_200, (b) SACNT_300, (c) SACNT_400, (d) Com_0.22, and (e) Com_0.45 membranes. (f) Comparison in terms of three surface Roughness parameter (i.e., R_{RMS}, R_{max}/10, and R_a) among these membranes.

3.2 Membrane surface functional groups

Fig. 4 presents a comparison of FTIR spectra among the SACNT and commercial PVDF membranes. As expected, the FTIR spectra of the SACNT membranes are similar, but dramatically different from those of the Com_0.22 and Com_0.45 membranes. No obvious absorption peak was observed in the SACNT spectra. This is because the SACNT membranes were prepared purely form CNTs. The hexagonal graphene structure of CNT has no obvious absorption of infrared waves. By contrast, several characteristic peaks were identified in the Com_0.22 and Com_0.45 spectra. The peak at ~1400 cm^{-1} is associated with the deformation and vibration of $–CH_2–$ that is connected with $–CF_2–$ (Xu et al., 2012). The ~1175 cm^{-1} peak should be owing to the stretching vibration of $–CF_2–$ (Xu et al., 2012). These groups correspond well with the chemistry of the PVDF matrix of the commercial membranes, and are also consistent with the EDS results in Fig. 2(f). The sharp 877 cm^{-1} peak can be ascribed to the vibration of crystalline phase in the membrane (Dizon et al., 2021). Besides, a small peak at ~1740 cm^{-1} relative to the vibration of –C=O was also identified (Rasekh and Raisi, 2021). This could be owing to some hydrophilic additives added during membrane fabrication. Overall, the FTIR analyses reveal that the SACNT membranes possess significantly simpler surface chemistry than the commercial PVDF membranes.

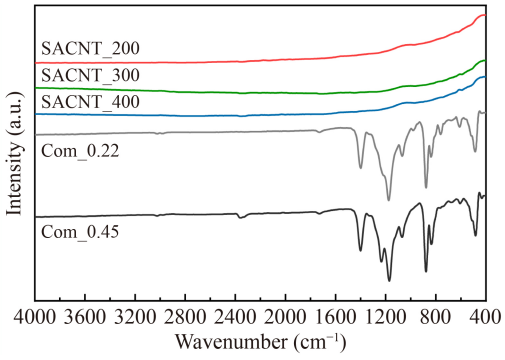

Fig. 4 Comparison of the FTIR spectra among the SACNT_200, SACNT_300, SACNT_400, Com_0.22 PVDF, and Com_0.45 PVDF membranes.

3.3 Unique nonpolar surface wetting behavior

Surface wetting behaviors of the membranes were investigated through a series of contact angle measurements. Two polar liquids (i.e., DI water and formamide) and one nonpolar liquid (i.e., diiodomethane) were separately used for the measurements.

In essence, the contact angle between the membrane and the liquid indicates the strength or affinity of their interactions (van Oss, 2006; Wang et al., 2017; Zhu et al., 2017). A lower contact angle suggests a stronger interaction or higher affinity. In the wastewater treatment filed where most substances are polar, most efforts for membrane modification have been made to increase membrane surface tensions (commonly by achieving

larger electronegativity to form a protective hydration layer (Tiraferri et al., 2012)), thereby resulting in smaller water contact angles thus enhanced hydrophilicity and antifouling performance (Wang et al., 2016; Seyed Shahabadi and Brant, 2019). But the polarity of molecules also determines the molecular interaction behavior (van Oss, 2006). The polar–polar interaction is normally strong and associated with high affinity. The nonpolar–nonpolar interaction is weak but with high affinity. The polar–nonpolar interaction is commonly weak and with low affinity. Therefore, considering the polar circumstances that a membrane normally faces in wastewater treatment, a nonpolar membrane may exhibit advantages in antifouling, because its near zero electric dipole moment is not conducive to the deposition of pollutants on the membrane surface (van Oss, 2003; 2007; Andersen et al., 2014).

As shown in Fig. 5, both the control commercial membranes (i.e., Com_0.22 and Com_0.45) exhibited a typical wetting behavior which was consistent with other previous studies (Han et al., 2019). The measured water contact angle for the Com_0.22 and Com_0.45 membranes are 66.8° ± 4.6° and 69.9° ± 2.3°, respectively. The measured formamide and diiodomethane contact angles are smaller, since the surface tensions of formamide and diiodomethane are lower than that of water.

In marked contrast, all the SACNT membranes exhibited much higher contact angles than the commercial membranes when facing polar liquids (i.e., water and formamide). The measured water contact angles of the SACNT_200, SACNT_300, and SACNT_400 membranes are 124.9° ± 3.2°, 126.5° ± 1.8°, and 126.5° ± 2.6°, respectively. It demonstrates the hydrophobic nature of the SACNT membranes. The measured formamide contact angles are 80.0° ± 5.4°, 83.9° ± 4.0°, and 82.4° ± 2.5°, respectively. These data are significantly higher than those of the commercial membranes.

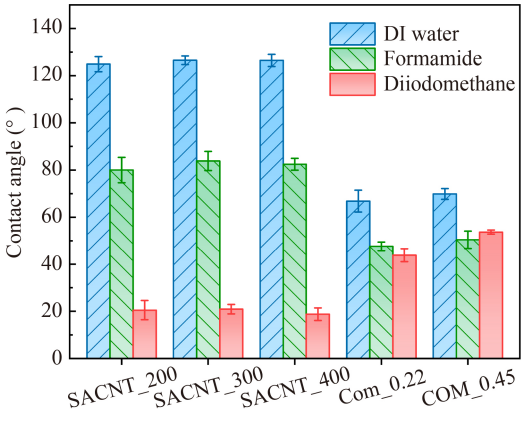

Fig. 5 Comparison of surface wetting behavior in terms of static contact angles measured with three different liquids (i.e., DI water, formamide, and diiodomethane) among the SACNT_200, SACNT_300, SACNT_400, Com_0.22, and Com_0.45 membranes.

However, when facing the nonpolar diiodomethane, the SACNT membranes showed dramatically lower contact angles (around 20°) than the commercial membranes, indicating a high affinity between them. This unique wetting behavior should be owing to the nonpolar nature of the CNTs. It is noteworthy that the wetting behaviors of the SACNT_200, SACNT_300, and SACNT_400 membranes are similar, indicating that stacking more SACNT layers does not change the final surface wetting behavior.

3.4 Superior permeability and selectivity

The filtration performance of the SACNT membranes was assessed in terms of water permeability and MWCO-based selectivity. Fig. 6(a) presents a comparison of measured water permeability among the membranes. As compared with the commercial membranes, the SACNT_200 membrane achieved a more than two times higher permeability (~14.4 × 10^{-6} m/(s·kPa)), but still maintained the higher rejection rates at all the tested molecular weights (Fig. 6(b)) in the MWCO tests. As the membrane technology is currently facing the challenge of "permeability–selectivity" trade-off effect (Zhang et al., 2020b; Sun et al., 2022b), the SACNT membranes prepared in this study surpass the commercial membranes

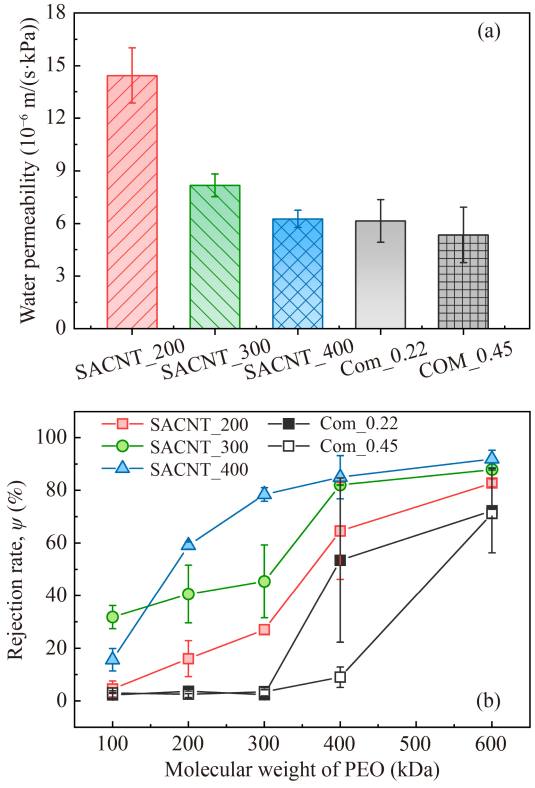

Fig. 6 Comparison of pure water permeability and selectivity in terms of molecular weight cutoff (MWCO) among the SACNT_200, SACNT_300, SACNT_400, Com_0.22, and Com_0.45 membranes.

with both superior permeability and selectivity, suggesting promising applications in the membrane filtration fields.

As discussed in the above sections, stacking more SACNT layers does not significantly affect surface properties (e.g., morphology, chemistry, and surface wetting). But it can be expected that more SACNT layers will bring about more filtration resistance. As shown in Fig. 6(a), a gradual permeability decrease was observed as the number of stacked SACNT layers increased. But correspondingly, an increase of rejection rates was also observed. The SACNT_400 membrane possesses a similar permeability with the commercial membranes, but achieved much higher rejection rates. The 90 % PEO rejection was achieved at ~550 kDa. The superior filtration performance of the SACNT membranes should be owing to the abundant and uniform interspace formed among the CNTs.

3.5 Nonpolar and conductive features endow SACNT membranes with superior antifouling capability

As discussed in Section 3.3, the nonpolar property of the SACNT membranes might result in improved antifouling performance owing to its low interfacial interaction forces with polar pollutants. Furthermore, the conductive feature of the SACNT also enables a potential of electro-assistant antifouling capability as reported previously (Li et al., 2020). In this study, we conducted two types of antifouling tests to investigate the antifouling behavior of the SACNT membranes. The Com_0.22 membrane was selected as a control for comparisons, since its selectivity is closer to those of the SACNT membranes than the Com_0.45 membrane.

Fig. 7(a) presents a comparison of the normalized flux decline curves among the membranes. In each filtration cycle, a flux decline was observed as the filtration started, indicating the development of membrane fouling. After about 10 min, the flux gradually reached a steady value, and the fluxes of the membranes generally followed an order of SACNT_200 > SACNT_300 > SACNT_400 > Com_0.22. This order also indicates the antifouling capability of the membranes. After the fouling stage, the membrane cleaning procedure was performed, and the calculated cleaning efficiency (η) was presented in Fig. 7(b). Although the different SACNT membranes

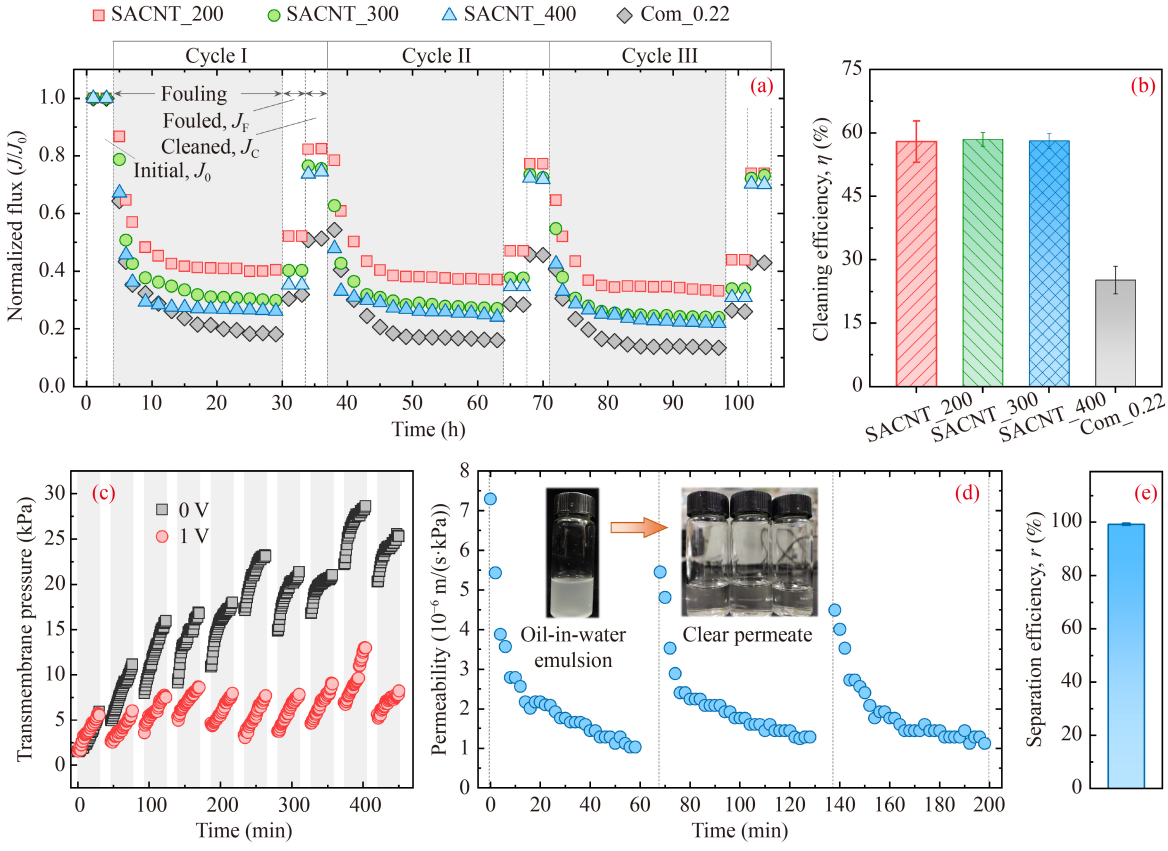

Fig. 7 (a) Comparison of membrane fouling behavior among the SACNT_200, SACNT_300, SACNT_400, and Com_0.22 membranes in the three-cycle filtration tests using the synthetic municipal wastewater (Table 1). (b) Comparison of calculated cleaning efficiency (η) in the three-cycle filtration tests. (c) Electro-assistant antifouling performance of the SACNT_200 membrane (as a representative). (d) Oil-water separation performance of the SACNT_200 membrane in the three-cycle separation test using oil-in-water emulsion. (e) Calculated separation efficiency in the three-cycle oil-water separation test.

maintained different fluxes during the fouling process (probably owing to their different filtration resistances), their cleaning efficiencies were found to be almost identical. This is reasonable because all the SACNT membranes possess similar surface properties. Furthermore, the calculated cleaning efficiencies of the SACNT membranes were >2.3 times higher than that of the Com_0.22 membrane, demonstrating superior antifouling performance. The better antifouling performance of the SACNT membranes could be owing to the smooth surface morphology (Fig. 3), unique nonpolar wetting property (Fig. 5), relatively inert surface chemistry (Fig. 4), and so forth.

Moreover, the SACNT_200 membrane was selected as a representative to evaluate the electro-assistant antifouling performance of the SACNT membranes. A set of electrically enhanced cross-flow filtration tests were performed in a constant flux mode. As shown in Fig. 7(c), in the 0 V test, quick TMP increases were observed in the ten-cycle tests as the filtration was started, indicating the fast development of membrane fouling. In marked contrast, when the 1 V voltage was applied to the filtration system (where the SACNT membrane served as a cathode), the TMP increase became significantly slower and the resulted TMP values are much lower than those in the 0 V tests. This improved antifouling capability can be ascribed to the applied electrophoretic force that could repulse foulants away from the membrane, and the possible electrocatalytic oxidation that could lead to the degradation of foulants (Li et al., 2020).

3.6 Superior oil/water separation performance

The interesting feature of the nonpolar SACNT membranes is that although it exhibits a hydrophobic and oleophilic wetting behavior in air (Fig. 5), it still exhibits an oleophobic wetting behavior in water. The underwater oil (soybean oil) contact angle of the SACNT_200 membrane is measured to be 132.8° ± 4.3°. This unique feature should be ascribed to the "hydrophobic" hydration effect of nonpolar surfaces (van Oss, 2006). Such a unique nonpolar property and its uniformly aligned porous structure (Fig. 2) endow the SACNT membrane with a capability for oil/water separation. As shown in Fig. 7(d), a three-cycle oil/water separation experiment using a stable emulsion (average particle size of 5.375 μm, Fig. S4) was conducted with the SACNT_200 membrane (as a representative). As a result, a high separation efficiency of > 99.2 % was constantly maintained in every filtration cycle with the permeate concentrations much lower than the discharge standard (10 mg/L, China GB 8978-1996), demonstrating a superior oil/water separation capability. It is noteworthy that a gradual decrease of flux was observed in all the filtration cycles. This could be owing to the oil-induced membrane fouling due to the high affinity between the SACNT membrane and oil particles (Shi et al., 2013).

Overall, the SACNT membranes exhibited superior separation performance in various application scenarios, including municipal wastewater treatment, electro-assistant fouling inhibition (or even self-cleaning), and oil/water separation, which suggests promising prospects of applications in various fields. But it is worth noting that the free-standing SANCT membranes are basically held by van der Waals forces. It has been demonstrated that the resulted entity is very strong (Wei et al., 2013), suggesting a good capability to withstand the physical impact in the water treatment processes. But considering the complex chemistry of some harsh wastewaters (e.g., industrial wastewater with extreme pH conditions) could cause potential deterioration to the SACNT membranes, their treatment performance for those more complicated application scenarios is still unknown. Besides, although the market price of CNT materials is fairly low now, further reducing the production cost of the SACNT membrane is a continuing concern for practical applications. Future research is still needed to address these application challenges.

4 Conclusions

This study proposed a novel nonpolar SACNT membrane, which was prepared with a layer-by-layer cross-stacking method using the nonpolar CNTs as raw materials. Through controlling the number of stacked SACNT layers, three kinds of SACNT membranes (i.e., SACNT_200, SACNT_300, and SACNT_400) were prepared. As compared with the two commercial PVDF membranes (i.e., Com_0.22 and Com_0.45), all the SACNT membranes achieved smoother and more uniform structures. The measured R_a values of the SACNT_200, SACNT_300, and SACNT_400 membranes are 67.0 ± 3.7, 73.8 ± 19.9, and 43.9 ± 2.9 nm, respectively, much smaller than those of the commercial membranes. Due to the hexagonal graphene structure of CNTs, the surface chemistry of the SACNT membranes is simple and inert, which potentially eliminates the covalent-bonding-induced membrane fouling. Besides, the SACNT membranes exhibited a typical nonpolar wetting behavior, with high contact angles for the polar liquids (~124.9°–126.5° for DI water; ~80.0°–83.9° for formamide) but low contact angles for the nonpolar diiodomethane (~18.8°–20.9°). This unique nonpolar feature could lead to weak interactions with polar substances. Furthermore, compared with the commercial membranes, all the SACNT membranes obtained a significantly higher selectivity while achieving a comparable permeability (SACNT_200) or significantly higher permeabilities (SACNT_300 and SACNT_400). Moreover, the SACNT membranes exhibited superior separation performance in various application scenarios,

including municipal wastewater treatment (> 2.3 times higher cleaning efficiency), electro-assistant fouling inhibition (or even self-cleaning), and oil/water separation (> 99.2% of separation efficiency), which suggests promising application prospects in various fields.

Acknowledgements The authors gratefully acknowledge the financial support from the Fundamental Research Funds for the Central Universities (No. 2021ZY76), the National Natural Science Foundation of China (No. 52170022), the special fund of State Key Joint Laboratory of Environment Simulation and Pollution Control (No. 20K02ESPCT), and the Beijing Municipal Education Commission through the Innovative Transdisciplinary Program "Ecological Environment of Urban and Rural Human Settlements (GJJXK210105)".

Electronic Supplementary Material Supplementary material is available in the online version of this article at https://doi.org/10.1007/s11783-023-1630-3 and is accessible for authorized users.

References

Abaie E, Xu L, Shen Y X (2021). Bioinspired and biomimetic membranes for water purification and chemical separation: a review. Frontiers of Environmental Science & Engineering, 15(6): 124

Andersen S M, Borghei M, Dhiman R, Ruiz V, Kauppinen E, Skou E (2014). Adsorption behavior of perfluorinated sulfonic acid ionomer on highly graphitized carbon nanofibers and their thermal stabilities. Journal of Physical Chemistry C, 118(20): 10814–10823

Dizon G V, Lee Y S, Venault A, Maggay I V, Chang Y (2021). Zwitterionic PMMA-r-PEGMA-r-PSBMA copolymers for the formation of anti-biofouling bicontinuous membranes by the VIPS process. Journal of Membrane Science, 618: 118753

Han B J, Liang S, Wang B, Zheng J Z, Xie X, Xiao K, Wang X M, Huang X (2019). Simultaneous determination of surface energy and roughness of dense membranes by a modified contact angle method. Colloids and Surfaces. A, Physicochemical and Engineering Aspects, 562: 370–376

Hand S, Cusick R D (2021). Electrochemical disinfection in water and wastewater treatment: Identifying impacts of water quality and operating conditions on performance. Environmental Science & Technology, 55(6): 3470–3482

Hu Y T, Lu Z H, Wei C, Yu S C, Liu M H, Gao C J (2018). Separation and antifouling properties of hydrolyzed PAN hybrid membranes prepared via in-situ sol-gel SiO_2 nanoparticles growth. Journal of Membrane Science, 545: 250–258

Ihsanullah (2019). Carbon nanotube membranes for water purification: developments, challenges, and prospects for the future. Separation and Purification Technology, 209: 307–337

Jia F C, Xiao X, Nashalian A, Shen S, Yang L, Han Z Y, Qu H J, Wang T M, Ye Z, Zhu Z J, Huang L J, Wang Y X, Tang J G, Chen J (2022). Advances in graphene oxide membranes for water treatment. Nano Research, 15(7): 6636–6654

Jiang J, Ma B Y, Yang C W, Duan X Y, Tang Q (2022). Fabrication of anti-fouling and photocleaning PVDF microfiltration membranes embedded with N-TiO_2 photocatalysts. Separation and Purification Technology, 298: 121673

Lee J H, Kim H S, Yun E T, Ham S Y, Park J H, Ahn C H, Lee S H, Park H D (2020). Vertically aligned carbon nanotube membranes: water purification and beyond. Membranes (Basel), 10(10): 273

Li M, Wu L, Zhang C, Chen W, Liu C (2019). Hydrophilic and antifouling modification of PVDF membranes by one-step assembly of tannic acid and polyvinylpyrrolidone. Applied Surface Science, 483: 967–978

Li M, Zuo K, Liang S, Xiao K, Liang P, Wang X, Huang X (2020). Electrically tuning ultrafiltration behavior for efficient water purification. Environmental Science & Technology, 54(18): 11536–11545

Li Y, Gao R, Zhang J, Zhang Y, Liang S (2022). Antifouling conductive composite membrane with reversible wettability for wastewater treatment. Membranes (Basel), 12(6): 626

Li Z, Lu L (2022). Wastewater treatment meets artificial photosynthesis: solar to green fuel production, water remediation and carbon emission reduction. Frontiers of Environmental Science & Engineering, 16(4): 53

Liu K, Sun Y, Liu P, Lin X, Fan S, Jiang K (2011). Cross-stacked superaligned carbon nanotube films for transparent and stretchable conductors. Advanced Functional Materials, 21(14): 2721–2728

Liu X, Tian C, Zhao Y, Xu W, Dong D, Shih K, Yan T, Song W (2022). Enhanced cross-flow filtration with flat-sheet ceramic membranes by titanium-based coagulation for membrane fouling control. Frontiers of Environmental Science & Engineering, 16(8): 110

Ma R H, Lu X L, Zhang S Z, Ren K, Gu J, Liu C, Liu Z Q, Wang H L (2022). Constructing discontinuous silicon-island structure with low surface energy based on the responsiveness of hydrophilic layers to improve the anti-fouling property of membranes. Journal of Membrane Science, 659: 120770

Ma Z, Liang S, Zhang S, Xiao K, Wang X, Li M, Huang X (2020). Surface functionalization via synergistic grafting of surface-modified silica nanoparticles and layered double hydroxide nanosheets for fabrication of superhydrophilic but relatively oleophobic antifouling membranes. Separation and Purification Technology, 247: 116955

Qin A W, Wu X L, Ma B M, Zhao X Z, He C J (2014). Enhancing the antifouling property of poly (vinylidene fluoride)/SiO_2 hybrid membrane through TIPS method. Journal of Materials Science, 49(22): 7797–7808

Racar M, Dolar D, Karadakić K, Čavarović N, Glumac N, Ašperger D, Košutić K (2020). Challenges of municipal wastewater reclamation for irrigation by MBR and NF/RO: physico-chemical and microbiological parameters, and emerging contaminants. Science of the Total Environment, 722: 137959

Rasekh A, Raisi A (2021). Electrospun nanofibrous polyether-block-amide membrane containing silica nanoparticles for water desalination by vacuum membrane distillation. Separation and Purification Technology, 275: 119149

Seyed Shahabadi S M, Brant J A (2019). Bio-inspired superhydrophobic and superoleophilic nanofibrous membranes for non-aqueous solvent and oil separation from water. Separation and Purification Technology, 210: 587–599

Shen Y, Xiao K, Liang P, Sun J, Sai S, Huang X (2012). Characterization of soluble microbial products in 10 large-scale

membrane bioreactors for municipal wastewater treatment in China. Journal of Membrane Science, 415–416(0): 336–345

Shi Z, Zhang W, Zhang F, Liu X, Wang D, Jin J, Jiang L (2013). Ultrafast separation of emulsified oil/water mixtures by ultrathin free-standing single-walled carbon nanotube network films. Advanced Materials, 25(17): 2422–2427

Su B, Tian Y, Jiang L (2016). Bioinspired interfaces with superwettability: from materials to chemistry. Journal of the American Chemical Society, 138(6): 1727–1748

Sun C, Lyu Q, Si Y, Tong T, Lin L C, Yang F, Tang C Y, Dong Y (2022a). Superhydrophobic carbon nanotube network membranes for membrane distillation: high-throughput performance and transport mechanism. Environmental Science & Technology, 56(9): 5775–5785

Sun F Y, Zeng H J, Tao S Y, Huang Y X, Dong W Y, Xing D Y (2022b). Nanofiltration membrane fabrication by the introduction of polyhedral oligomeric silsesquioxane nanoparticles: feasibility evaluation and the mechanisms for breaking "trade-off" effect. Desalination, 527: 115515

Tiraferri A, Kang Y, Giannelis E P, Elimelech M (2012). Superhydrophilic thin-film composite forward osmosis membranes for organic fouling control: fouling behavior and antifouling mechanisms. Environmental Science & Technology, 46(20): 11135–11144

van Oss C J (2003). Long-range and short-range mechanisms of hydrophobic attraction and hydrophilic repulsion in specific and aspecific interactions. Journal of Molecular Recognition, 16(4): 177–190

Van Oss C J (2006). Interfacial Forces in Aqueous Media. New York: Taylor & Francis

van Oss C J (2007). Development and applications of the interfacial tension between water and organic or biological surfaces. Colloids and Surfaces. B, Biointerfaces, 54(1): 2–9

Wang B, Zhang Y, Zhang L (2017). Selective surface tension induced patterning on flexible textiles via click chemistry. Nanoscale, 9(14): 4777–4786

Wang M, Wang J, Jiang J W (2022). Membrane fouling: Microscopic insights into the effects of surface chemistry and roughness. Advanced Theory and Simulations, 5(1): 2100395

Wang R, Chen J, Chen L, Ye Z, Wu C, Gao W, Xie L, Ying Y (2020). Ultrathin and ultradense aligned carbon nanotube membranes for water purification with enhanced rejection performance. Desalination, 494: 114671

Wang Z, Elimelech M, Lin S (2016). Environmental applications of interfacial materials with special wettability. Environmental Science & Technology, 50(5): 2132–2150

Wei H, Wei Y, Wu Y, Liu L, Fan S, Jiang K (2013). High-strength composite yarns derived from oxygen plasma modified super-aligned carbon nanotube arrays. Nano Research, 6(3): 208–215

Wei S, Du L, Chen S, Yu H, Quan X (2021). Electro-assisted CNTs/ceramic flat sheet ultrafiltration membrane for enhanced antifouling and separation performance. Frontiers of Environmental Science & Engineering, 15(1): 11

Xiao K, Liang S, Wang X, Chen C, Huang X (2019). Current state and challenges of full-scale membrane bioreactor applications: a critical review. Bioresource Technology, 271: 473–481

Xiong S, Qian X F, Zhong Z X, Wang Y (2022). Atomic layer deposition for membrane modification, functionalization and preparation: a review. Journal of Membrane Science, 658: 120740

Xu C Q, Huang W, Lu X, Yan D Y, Chen S T, Huang H (2012). Preparation of PVDF porous membranes by using PVDF-g-PVP powder as an additive and their antifouling property. Radiation Physics and Chemistry, 81(11): 1763–1769

Yang Y, Qiao S, Zheng M, Zhou J, Quan X (2019). Enhanced permeability, contaminants removal and antifouling ability of CNTs-based hollow fiber membranes under electrochemical assistance. Journal of Membrane Science, 582: 335–341

Zhang H, Quan X, Chen S, Yu H, Niu J (2020a). Electrokinetic enhancement of water flux and ion rejection through graphene oxide/carbon nanotube membrane. Environmental Science & Technology, 54(23): 15433–15441

Zhang Z, Li S, Mi B, Wang J, Ding J (2020b). Surface slip on rotating graphene membrane enables the temporal selectivity that breaks the permeability-selectivity trade-off. Science Advances, 6(34): eaba9471

Zhao X T, Zhang R N, Liu Y N, He M R, Su Y L, Gao C J, Jiang Z Y (2018). Antifouling membrane surface construction: chemistry plays a critical role. Journal of Membrane Science, 551: 145–171

Zhao Y, Zhao Y, Yu X, Kong D, Fan X, Wang R, Luo S, Lu D, Nan J, Ma J (2022). Peracetic acid integrated catalytic ceramic membrane filtration for enhanced membrane fouling control: performance evaluation and mechanism analysis. Water Research, 220: 118710

Zhu K, Luo Y, Zhao F, Hou J, Wang X, Ma H, Wu H, Zhang Y, Jiang K, Fan S, Wang J, Liu K (2018). Free-standing, binder-free titania/super-aligned carbon nanotube anodes for flexible and fast-charging Li-ion batteries. ACS Sustainable Chemistry & Engineering, 6(3): 3426–3433

Zhu Z, Zheng S, Peng S, Zhao Y, Tian Y (2017). Superlyophilic interfaces and their applications. Advanced Materials, 29(45): 1703120

Zin G, Wu J J, Rezzadori K, Petrus J C C, Di Luccio M, Li Q L (2019). Modification of hydrophobic commercial PVDF microfiltration membranes into superhydrophilic membranes by the mussel-inspired method with dopamine and polyethyleneimine. Separation and Purification Technology, 212: 641–649